J Electr Eng Technol Vol. 8, No. 4: 879-888, 2013
http://dx.doi.org/10.5370/JEET.2013.8.4.879

ISSN(Print) 1975-0102
ISSN(Online) 2093-7423

3D Vision-Based Local Path Planning System of a Humanoid Robot for Obstacle Avoidance

Tae-Koo Kang*, Myo-Taeg Lim*, Gwi-Tae Park* and Dong W. Kim†

Abstract – This paper addresses the vision based local path planning system for obstacle avoidance. To handle the obstacles which exist beyond the field of view (FOV), we propose a Panoramic Environment Map (PEM) using the MDGHM-SIFT algorithm. Moreover, we propose a Complexity Measure (CM) and Fuzzy logic-based Avoidance Motion Selection (FAMS) system to enable a humanoid robot to automatically decide its own direction and walking motion when avoiding an obstacle. The CM provides automation in deciding the direction of avoidance, whereas the FAMS system chooses the avoidance path and walking motion, based on environment conditions such as the size of the obstacle and the available space around it. The proposed system was applied to a humanoid robot that we designed. The results of the experiment show that the proposed method can be effectively applied to decide the avoidance direction and the walking motion of a humanoid robot.

Keywords: Local path planning, MDGHM-SIFT, Complexity measure, Humanoid robot, Avoidance motion selection

1. Introduction

Humanoid robotics has recently become an active area of research and development as well as many related studies, such as autonomous walking, avoiding obstacles, stepping over obstacles, and walking up and down slopes and stairs.

Yagi and Lumelsky [1] presented an experiment where the robot adjusts the length of its steps until it reaches an obstacle, depending on the distance between the robot and the nearest obstacle in the robot's direction of motion. If the size of the obstacle is small, the robot steps over the obstacle. If the obstacle is too tall, the robot sidesteps until it clears the obstacle. Obviously, the decision whether to sidestep left or right is also a preprogrammed one. Kuffner et al. [2] presented a footstep-planning algorithm based on game theory, which takes into account the position of the obstacles in the environment. Chestnutt et al. [3] and Michel et al. [4] presented their vision-guided footstep planning algorithm to avoid obstacles, using Honda's ASIMO robot. These systems get an overhead view of the environment from a camera or a sensor installed above the humanoid robot. Stasse et al. [5] and Kanehiro et al. [6] presented a stereovision-based locomotion planning algorithm, which can modify the robot's waist height and upper body posture, according to the size of the available space. Ayaz et al. [7] suggested the footstep planning algorithm, which is more suited to cluttered environments, depending on the obstacle's properties. Finally, Gutmann et al. [8] suggested a modular architecture with the perception layer, the control layer, and the planning layer for use in humanoid robot navigation.

In this paper, we focus on obstacle avoidance using a 3D-vision system. In particular, we address the Field of View (FOV) problem and external path planner problem. The FOV problem occurs whenever a humanoid robot encounters an obstacle that is too large, thereby preventing it from precisely estimating the obstacle's size and from deciding the appropriate motion. Therefore, we propose a MDGHM-SIFT-based Panoramic Environment Map (PEM) to estimate the size of the large obstacles.

In addition, external path planners, which provide information regarding the walking path and obstacles, have been used in guiding the humanoid robots to the pre-defined target position [3, 8]. However, the path planner does not necessarily know in advance all information about the walking environment, particularly, if the humanoid robot is in an unknown environment. To overcome these problems, we propose a system that combines Complexity Measure (CM) and Fuzzy logic-based Avoidance Motion Selection (FAMS). The CM calculates the complexity of different the avoidance direction so that a humanoid robot can automatically decide which direction to take to avoid the obstacle. The FAMS system also chooses the avoidance motion of the humanoid robot based on obstacle information. Finally, the rotation that the robot has to turn and the distance that it has to span are calculated using the environment information extracted from PEM.

This paper is organized as follows: In Chapter 2, we introduce the vision-based local path planning system. In Chapter 3, we provide the results of experiments that

† Corresponding Author: Dept. of Digital Electronics and Information Engineering, Inha Technical College, Korea. (dwnkim @inhatc.ac.kr)
* School of Electrical Engineering, Korea University, Korea. ({tkkang, mlim, gtpark}@korea.ac.kr)
Received: September 9, 2012; Accepted: February 26, 2013

focused on the performances of the proposed system. Chapter 4 presents our contributions.

2. Detailed Formats of Manuscript

We propose a 3D vision-based local path planning system that uses a 3D panoramic environment map (PEM), extracts environment information, and decides on avoidance direction and motion. The methods are presented in detail blow.

2.1 Architecture of overall system

The overall local environment recognition system architecture is illustrated in Fig. 1.

The system consists of three general parts: 1) 3D PEM generation, 2) extraction of environment information and selection of avoidance direction, and 3) selection of avoidance motion. In the 3D PEM generation part, we use a MDGHM-SIFT algorithm that we have proposed in [10] to improve the matching accuracy. In [15], the SIFT shows the sensitivity for large rotation change and large viewpoint change conditions. The MDGHM-SIFT algorithm is a modification version of the orientation assignment stage in the SIFT algorithm. In [10], the MDGHM-SIFT outperforms the existing SIFT relative algorithms in terms of large rotation change and large viewpoint change by replacing the gradient method. The MDGHM-SIFT-based PEM generation provides more precise information about the environment than other versions of the SIFT.

During the extraction of environment information and selection of avoidance direction, we determine the environment information, including distances and angles between the robot and the obstacles, as well as the sizes of the obstacles. In addition, we propose a Complexity Measure (CM) method to select the avoidance direction.

In selecting the avoidance motion, we propose new methods using environment information and fuzzy logic.

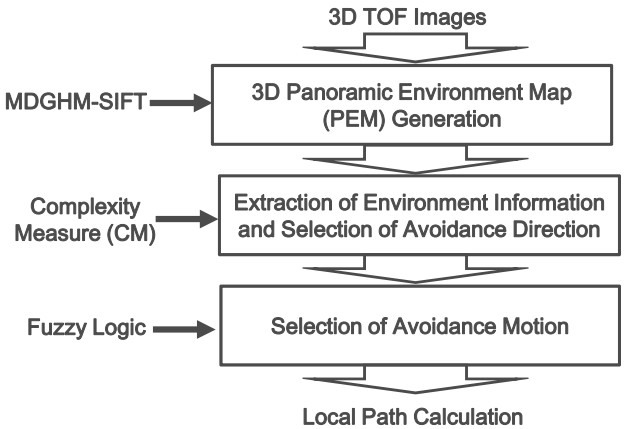

Fig. 1. Overview of the local path planning system.

2.2 Abstract and keywords

2.2.1 MDGHM-SIFT review

The DGHM is a global feature method that represents a square image in discrete domain [9]. DGHM cannot be applied to non-square images because the discrete Gaussian-Hermite functions might cause image data loss (image truncation) or require extra computation [10].

The MDGHM [10] is the modified version of the DGHM using a mask. To improve the accuracy of the environment information, we used the MDGHM in place of a gradient method at the third stage (orientation assignment) of the conventional SIFT algorithm, which is a local feature algorithm. The resulting algorithm is the MDGHM-SIFT.

Let $I(i,j)$ be a digital 2D image whose size is $W \times H$ $[0 \le i \le W-1, 0 \le j \le H-1]$, and let $t(u,v)$ be a mask whose size is $M \times N$ $[0 \le u \le M-1, 0 \le v \le N-1]$.

In [9], Gaussian-Hermite functions are obtained as follows:

$$\begin{cases} \bar{H}_p(x,\sigma) = \dfrac{2}{K-1}\dfrac{1}{\sqrt{2^p\, p!\sqrt{\pi}\sigma}}\exp(-x^2/2\sigma^2)H_p(x/\sigma) \\ \bar{H}_q(y,\sigma) = \dfrac{2}{K-1}\dfrac{1}{\sqrt{2^q\, q!\sqrt{\pi}\sigma}}\exp(-y^2/2\sigma^2)H_q(y/\sigma) \end{cases} \quad (1)$$

From the (1), DGHM can be derived as follows:

$$\eta_{p,q} = \frac{4}{(K-1)^2}\sum_{i=0}^{K-1}\sum_{j=0}^{K-1} I(i,j)\,\bar{H}_p(x,\sigma)\,\bar{H}_q(y,\sigma). \quad (2)$$

To convert DGHM to MDGHM, we define the number of maximum samples, k_M, k_N, as follows:

$$k_M = M/m_M,\ k_N = N/m_N,\ \text{for } t(u,v) \quad (3)$$

where m_M and m_N are sampling intervals on the u-*axis* and v-*axis* respectively. The pixel values of the mask $t(u,v)_{(i,j)}$ located at an arbitrary point (i,j) on the input image $I(i,j)$ are obtained as follows:

$$t(u,v)_{(i,j)} = I(u+i-M/2+1, v+j-N/2+1) \quad (4)$$

For the mask $t(u,v)_{(i,j)}$, the coordinate is transformed to be $-1 \le x, y \le 1$ as follows:

$$x = \frac{2u-M+1}{M-1},\quad y = \frac{2v-N+1}{N-1} \quad (5)$$

and the MDGHM functions of the mask $t(u,v)_{(i,j)}$ can be written as follows:

$$\begin{cases} \hat{H}_p(x,\sigma) = \dfrac{2}{M-1}\bar{H}_p(x/\sigma) \\ \quad = \dfrac{2}{M-1}\dfrac{1}{\sqrt{2^p p!\sqrt{\pi}\sigma}}\exp(-x^2/2\sigma^2)H_p(x/\sigma) \\ \hat{H}_q(y,\sigma) = \dfrac{2}{N-1}\bar{H}_q(y/\sigma) \\ \quad = \dfrac{2}{N-1}\dfrac{1}{\sqrt{2^q q!\sqrt{\pi}\sigma}}\exp(-y^2/2\sigma^2)H_q(y/\sigma) \end{cases} \quad (6)$$

where p and q are the orders of the MDGHM function and σ represents the standard deviation.

From (4) and (6), the MDGHM with sampling intervals at the arbitrary point (i,j) on the input image $I(i,j)$ can be written as follows:

$$\hat{\eta}_{p,q}(i,j,m_M,m_N) = \frac{4}{(M-1)(N-1)}\sum_{u=0}^{k_M-1}\sum_{v=0}^{k_N-1} I(i+(m_M u - M/2+1), j+(m_N v - N/2+1)) \hat{H}_p(x,\sigma)\hat{H}_q(y,\sigma). \quad (7)$$

The MDGHM-based magnitude $\hat{m}(i_a, j_a, s)$ and orientation $\hat{\mu}(i_a, j_a, s)$, of the SIFT are as follows:

$$\hat{m}(i_a,j_a,s) = \sqrt{\sum_{p=0}^{2}(\hat{\eta}_{(2p+1),0}(i_a,j_a,s))^2 + \sum_{q=0}^{2}(\hat{\eta}_{0,(2q+1)}(i_a,j_a,s))^2}, \quad (8)$$

$$\hat{\mu}(i_a,j_a,s) = \arctan\left(\frac{\sqrt{\sum_{q=0}^{2}(\hat{\eta}_{0,(2q+1)}(i_a,j_a,s))^2}}{\sqrt{\sum_{p=0}^{2}(\hat{\eta}_{(2p+1),0}(i_a,j_a,s))^2}}\right). \quad (9)$$

In (6), the size of the MDGHM is defined as:

$$\begin{cases} M = 2\times round(\max(p)\sigma)+1 & \text{for } x\text{-axis} \\ N = 2\times round(\max(q)\sigma)+1 & \text{for } y\text{-axis} \end{cases} \quad (10)$$

2.2.2 MDGHM-SIFT-Based PEM generation

To solve the FOV problem, where humanoid robots cannot precisely estimate the size of very large obstacles, we generate the Panoramic Environment Map (PEM) using MDGHM-SIFT [10]. Table 1 shows the procedure of PEM generation.

The first five steps are similar to conventional SIFT-based panoramic image generation [12]. However, we use the MDGHM-SIFT algorithm in the remaining steps to match features more precisely. Since MDGHM-SIFT features are less sensitive under scale, rotation, viewpoint, and illumination changes than those of the traditional SIFT, our system can handle images with varying orientation and zoom settings.

Fig. 2 shows a result of the PEM using depth images gathered from a Time-of-Flight (TOF) camera installed on a humanoid robot when the robot is standing in front of the obstacles. From the PEM, we obtained the environment

Table 1. Algorithm: 3D PEM Generation.

Algorithm: 3D Panoramic Environment Map
Input : n unordered images Output : 3D PEM image
Sequence: - Extract MDGHM-SIFT features of all n depth images - Select m candidate matching pairs having the most features. - Find geometrically consistent feature matches using RANSAC. - Perform bundle adjustment. - Render 3D panoramic image using multi-band blending. - Find key angular positions on the 3D panoramic image using FNCC. - Find all angular positions (θ, ϕ) using linear interpolation.

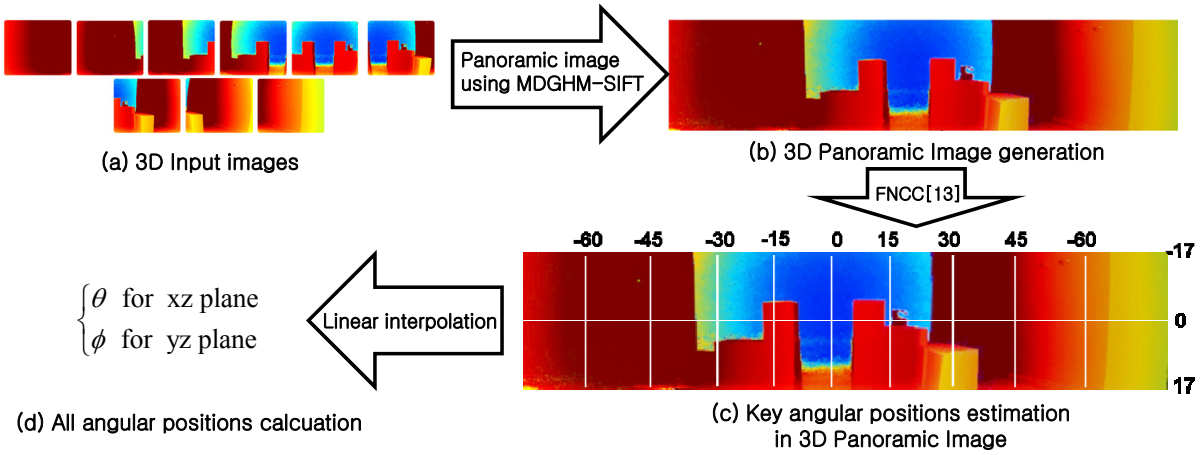

Fig. 2. The PEM image result: (a) nine input images obtained from 3D TOF camera installed on the Humanoid Robot, (b) 3D panoramic image; (c) key angular positions estimation; (d) all angular positions calculation.

information, such as size of the obstacle, the locations of obstacle, and the distance between the robot and the obstacle.

Let θ and ϕ be rotation angles onto xz and yz plane respectively. In Fig. 2, the key angular positions for each pixel can be estimated using Fast Normalized Cross Correlation (FNCC) [13] as follows:

$$\gamma(u,v)=\frac{\sum_{x,y}\left[f(x,y)-\overline{f_{u,v}}\right]\left[t(x-u,y-v)-\bar{t}\right]}{\left\{\sum_{x,y}\left[f(x,y)-\overline{f_{u,v}}\right]^2\left[t(x-u,y-v)-\bar{t}\right]^2\right\}^{0.5}} \quad (11)$$

where f is the 3D panoramic image, t is an input depth image from the 3D TOF camera, $\bar{t}$ is the mean of the t, $\overline{f_{u,v}}$ is the mean of $f(x,y)$ in the region under the depth image t respectively. The FNCC calculates the similarity between the 3D panoramic image and input 3D TOF images, and finds the most similar position. Each result is an estimated point (x, y), where x is considered the horizontal angular position from -60 to 60 degree with an interval of 30 degrees and y is the vertical angular position from -17 to 17 degree with an interval of 17 degrees. Fig. 2(c) shows the result of the key angular position estimation.

From the key angle positions, all angular positions on the PEM are calculated using linear interpolation as follows:

$$\theta=\begin{cases}\mathbf{A}_i+\dfrac{(\mathbf{A}_{i+1}-\mathbf{A}_i)\times(x-x_{A_i})}{(x_{\mathbf{A}_{i+1}}-x_{\mathbf{A}_i})}, & \mathbf{A}_{i+1}>\mathbf{A}_i>0\\ \mathbf{A}_i-\dfrac{(\mathbf{A}_i-\mathbf{A}_{i+1})\times(x_{\mathbf{A}_i}-x)}{(x_{\mathbf{A}_i}-x_{\mathbf{A}_{i+1}})}, & 0<\mathbf{A}_{i+1}<\mathbf{A}_i\end{cases}$$
$$\phi=\begin{cases}\mathbf{B}_i+\dfrac{(\mathbf{B}_{i+1}-\mathbf{B}_i)\times(y-y_{\mathbf{B}_i})}{(y_{\mathbf{B}_{i+1}}-y_{\mathbf{B}_i})}, & \mathbf{B}_{i+1}>\mathbf{B}_i>0\\ \mathbf{B}_i-\dfrac{(\mathbf{B}_i-\mathbf{B}_{i+1})\times(y_{\mathbf{B}_i}-y)}{(y_{\mathbf{B}_i}-y_{\mathbf{B}_{i+1}})}, & 0<\mathbf{B}_{i+1}<\mathbf{B}_i\end{cases} \quad (12)$$

where, $\mathbf{A}=\{-60,-30,0,30,60\}$ and $\mathbf{B}=\{-17,0,17\}$. In (12), $x_{\mathbf{A}_i}$ and $x_{\mathbf{A}_{i+1}}$ represent positions on the x-*axis* for the key angle $\mathbf{A}_i$ and $\mathbf{A}_{i+1}$ respectively.

2.3 Extraction of environment information and selection of avoidance direction

From the PEM, we can locate the obstacles and determine their environment information such as size of the obstacle, location, and distance from the robot.

First of all, division of the level sets is needed to extract the obstacle according to the distance. Let $I(x_i,y_i,z_i)$, $i=1,\ldots,N$ be a 3D panoramic image with N pixels. The level set is divided into m bins. The number of bins affects the interval between each level set. In our case, we define the maximum available distance $d_{\max}$ =2.5m and the total bins for level set m =50. Based on the distance of each pixel z from the camera, the level set is defined as follows:

$$level\ set(I_k)=\begin{cases}I_k(x^k,y^k,z^k)\leftarrow I(x,y,z) & \text{k=j}\\ 0 & \text{else}\end{cases} \quad (13)$$

where $k=1,\ldots,m$, $j=floor(floor(z)/\Delta d)$, $\Delta d=d_{\max}/m$. If $k=1$, it means that the point's distance from the robot is less than 5cm.

In order to identify the obstacles in the level set, we have to detect the blob in the 3D PEM. Blob detection is performed by the Connected Component Labeling (CCL) algorithm [16]. From the level set, obstacles are indexed by CCL as follow:

$$\mathbf{o}_l^k(\phi_l^k,\theta_l^k,d_l^k,w_l^k,h_l^k)=CCL(I_k(x_i^k,y_i^k,z_i^k)) \quad (14)$$

In (14), o_l^k means the l th object or obstacle in the k th level set extracted by CCL. These indexed obstacles are used as the input data for the selection of avoidance direction and for obstacle analysis. The parameters of o_l^k are calculated as illustrated in Fig. 3. The rotation angles ϕ_l^k,θ_l^k from the robot's current direction to the center of the obstacle o_l^k are obtained from the PEM directly. Therefore, we can calculate the perpendicular distance d_l^k from the robot to the obstacle o_l^k as follows:

$$d_l^k=z_l^k\cos\theta_l^k \quad (15)$$

From (15), maximum width w_{FOV} and maximum height h_{FOV} for FOV according to the perpendicular distance d_l^k are calculated as follows:

$$w_{FOV}=2\times\tan(\theta_{FOV}/2)\times d_l^k \quad (16)$$
$$h_{FOV}=2\times\tan(\phi_{FOV}/2)\times d_l^k \quad (17)$$

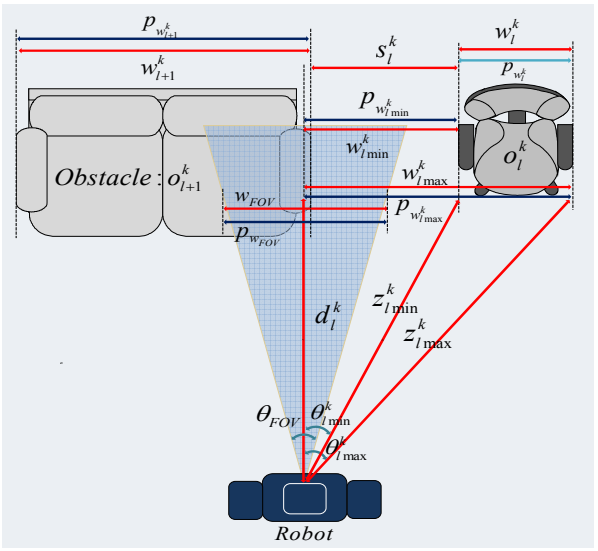

Fig. 3. Obstacle analysis: location and size calculation.

From (16) and (17), the width and height of obstacles w_l^k are calculated as follows:

$$w_l^k = w_{FOV} \times (\#p_{w_l^k} / \#p_{w_{FOV}}) \tag{18}$$

$$h_l^k = h_{FOV} \times (\#p_{h_l^k} / \#p_{h_{FOV}}) \tag{19}$$

where $\#p_{w_l^k}$ and $\#p_{h_l^k}$ represent the number of pixel points for width and height of the obstacle $\mathbf{o}_l^k$.

Moreover, from (18), the avoidance space s_l^k between obstacles can be calculated as follows:

$$s_l^k = \begin{cases} \left| w_{l\min}^k - w_{(l+1)\max}^k \right| & \text{for } \theta_l^k > 0,\ \theta_{l+1}^k > 0 \\ \left| w_{(l+1)\min}^k - w_{l\max}^k \right| & \text{for } \theta_l^k < 0,\ \theta_{l+1}^k < 0 \\ \left| w_{l\min}^k + w_{(l+1)\min}^k \right| & \text{for } \theta_l^k > 0,\ \theta_{l+1}^k < 0 \end{cases} \tag{20}$$

Environment information obtained from obstacle analysis is used as the input data to decide the direction to take to avoid an obstacle. To select the avoidance direction, we define the Complexity Measure (CM) as follows:

$$CM = \begin{cases} \sum_{k=1}^{m} \sum_{l=1}^{n} \frac{1}{k} (2^{(\pi/2-\theta_l^k)} + w_l^k + h_l^k), & \theta_l^k > 0 \\ -\sum_{k=1}^{m} \sum_{l=1}^{n} \frac{1}{k} (2^{(\pi/2+\theta_l^k)} + w_l^k + h_l^k), & \theta_l^k < 0 \\ \sum_{k=1}^{m} \sum_{l=1}^{n} \frac{1}{k} (w_l^k + h_l^k), & \theta_l^k = 0 \end{cases} \tag{21}$$

As shown in (21), the CM is determined by three factors: the distance between the robot and the obstacle, the width and the height of the obstacle, and the angle of the obstacle from the robot's current direction. The CM has a large value in cases where the robot is close to the obstacle, where the angle from the center of the PEM to the obstacle is small, and where the obstacle is large in size. The larger CM value indicates that the environment is too complex for the robot to avoid the obstacles. From (21), we make the final selection using D as follows:

$$D = sign\left(\sum_{all\ obstacle} CM \right) = \begin{cases} D > 0, & \text{turn left} \\ D < 0, & \text{turn right} \end{cases} \tag{22}$$

The avoidance direction is decided by the summation of all CMs for all obstacles. In (22), the CMs for obstacles located on the left side of the robot have negative values, and the CMs for obstacles located on the right side of the robot have positive values. Therefore, if the D is a positive value, the robot turns to the left, and if the D is a negative value, the robot turns to the right.

2.4 Selection of avoidance motion

After choosing the direction to take to avoid the obstacle, motion type must be selected based on the environment conditions. To achieve this purpose, we need an intelligent control approach. The fuzzy system is one such approach that does not require mathematical model and has the ability to approximate nonlinear systems. In addition, it can be easily implemented and extended without computational cost. Therefore, we propose the Fuzzy Logic-based Motion Selection (FAMS) method.

In order to conduct the fuzzification, we define two input variables: 1) the difference of width w_i between the width of the obstacle w_l^k and the width of the robot w_r, and 2) the spatial difference s_i between the width of the avoidance space s_l^k and the width of the robot w_r.

$$\begin{aligned} w_i &= \left| w_l^k - w_r \right| \\ s_i &= \left| s_l^k - w_r \right| \end{aligned} \tag{23}$$

From (23), we define the input and output membership function of the fuzzy logic as shown in Fig. 4. The term sets of the input and output variables are selected as follows:

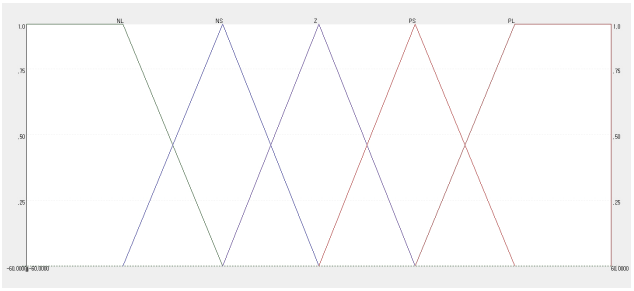

(a)

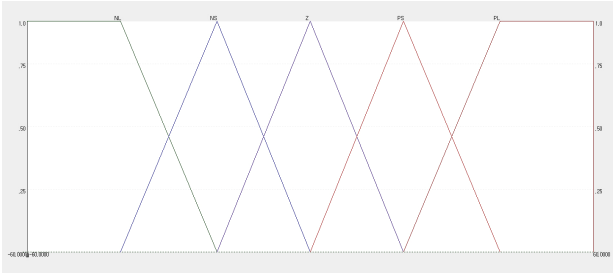

(b)

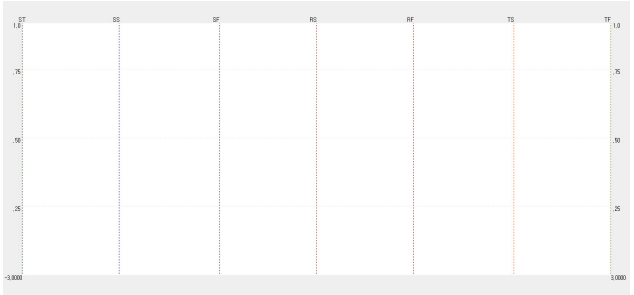

(c)

Fig. 4. Membership functions of fuzzy system: (a) Input variable w_i; (b) input variable s_i; (c) output variable f_i.

$$T(w_i)=\{A_1,A_2,A_3,A_4,A_5\}=\{NL,NS,Z,PS,PL\},$$
$$T(s_i)=\{B_1,B_2,B_3,B_4,B_5\}=\{NL,NS,Z,PS,PL\},$$
$$T(f_i)=\{C_1,C_2,C_3,C_4,C_5,C_6,C_7\}$$
$$=\{ST,SS,SF,RS,RF,TS,TF\}. \quad (24)$$

where fuzzy sets A_1, A_2, A_3, A_4, and A_5 are respectively denoted as Negative Large (NL), Negative Small (NS), Zero (Z), Positive Small (PS), Positive Large (PL) for the input variable w_i. Fuzzy sets B_1, B_2, B_3, B_4, and B_5 are also respectively denoted as Negative Large (NL), Negative Small (NS), Zero (Z), Positive Small (PS), Positive Large (PL) for the input variable s_i. Fuzzy sets $C_1, C_2, C_3, C_4, C_5, C_6$ and C_7 are respectively denote as Stop (ST), Slip step + Slip step (SS), Slip step + Forward step (SF), Rotation step + Slip step (RS), Rotation step + Forward step (RF), Turning step + Slip step (TS), and Turning step + Forward step (TF) which are two-motion combinations of Slip step (S), Forward step (F), Rotation step (R), Turning step (T) (except the Stop motion (ST) for the output variable f_i).

As shown in Fig. 4, each input variable is divided into five subsets, so that two inputs will construct 25 fuzzy rules. Moreover, output membership function of fuzzy logic determining the walking motion type corresponds to seven avoidance motion types. Table 2 and (25) describe the fuzzy rule base and rule table used in the proposed FAMS system.

$$\begin{aligned}&\text{Rule}\quad R(j_1,j_2):\\ &\text{IF } w_i \text{ is } A_{j_1} \text{ and } d_i \text{ is } B_{j2}, \text{ then } f_i \text{ is } C_{f(j_1,j_2)}\\ &j_1\in\{1,2,3,4,5\},\ j_2\in\{1,2,3,4,5\},\ f(j_1,j_2)\\ &\qquad\qquad\in\{1,2,3,4,5,6,7\}\end{aligned} \quad (25)$$

Table 2. Fuzzy rule table for FAMS.

f_i		s_i				
		NL	NS	Z	PS	PL
w_i	NL	ST	SS	SF	SF	SF
	NS	ST	SS	SF	SF	SF
	Z	ST	RS	RF	RF	RF
	PX	ST	RS	RF	RF	RF
	PL	ST	M	TF	TF	TF

To determine the final output of the FAMS system, we use the weighted average method described by

$$f_i=f(w_i,s_i)=\frac{\sum_{j_1=1}^{j_1=5}\sum_{j_2=1}^{j_2=5}u(j_1,j_2)\bullet v(C_{f(j_1,j_2)})}{\sum_{j_1=1}^{j_1=5}\sum_{j_2=1}^{j_2=5}u(j_1,j_2)} \quad (26)$$

where $v(C_{f(j_1,j_2)})$ is the crisp value of the fuzzy set, $C_{f(j_1,j_2)}$. The fire strength $u(j_1,j_2)$ of the rule $R(j_1,j_2)$ can be described by

$$u(j_1,j_2)=\min(\mu_{A_{j_1}}(w_i),\ \mu_{B_{j_2}}(s_i)) \quad (27)$$

Based on the w_i and s_i, seven evaluation values f_i, $i\in\{1,2,3,4,5,6,7\}$ for seven avoidance motions can be determined by the FAMS system. The selected avoidance motion type is one of seven motion types.

Finally, the local motion is planned using extracted environment information, the selected avoidance direction, and the selected avoidance motion. After the avoidance direction and the avoidance motion are determined, we decide the *pivot point*, which is the position where the robot changes its direction. Therefore, we calculate the distance d_{pivot} and the rotation angle θ_{pivot} from the robot's current position to the pivot point. In the case of RS and RF, we need two variables: 1) the moving distance, d_{pivot} from the robot's current position to the pivot point, and 2) the rotation angle, θ_{pivot} between the robot's current direction and the pivot point. These two variables are calculated as follows:

$$d_{pivot}=\begin{cases}\sqrt{(|w^k_{l\min}-s^k_l/2|)^2+(|d^k_l-s^k_l|)^2} & \text{for}\quad D<0\\ \sqrt{(|w^k_{(l+1)\min}-s^k_l/2|)^2+(|d^k_l-s^k_l|)^2} & \text{for}\quad D>0\end{cases} \quad (28)$$

$$\theta_{pivot}=\begin{cases}\arctan\left(\dfrac{|d^k_l-s^k_l|}{|w^k_{l\min}-s^k_l/2|}\right) & \text{for}\quad D<0\\ \arctan\left(\dfrac{|d^k_l-s^k_l|}{-|w^k_{(l+1)\min}-s^k_l/2|}\right) & \text{for}\quad D>0\end{cases} \quad (29)$$

In the case of SS and SF, the rotation angle is fixed at 0 degree, and in the case of TS and TF, the rotation angle is fixed at $\pm$ 180 degrees. Therefore, we don't need the calculation for the rotation angle. We just calculate the distance that the robot must traverse d_{pivot} as follows:

$$d_{pivot}=\begin{cases}|w^k_{l\min}-s^k_l/2| & \text{for } D<0\\ |w^k_{(l+1)\min}-s^k_l/2| & \text{for } D>0\end{cases}. \quad (30)$$

Thus, the robot can avoid obstacles automatically by using (28), (29), and (30).

3. Experimental Results

3.1 Humanoid robot design

To conduct the experiment, we designed and implemented a humanoid robot as shown in Fig. 5.

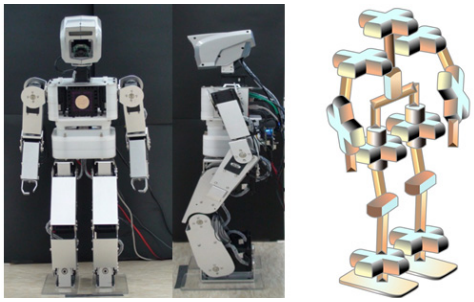

Fig. 5. The designed humanoid robot system.

Table 3. Specification of our humanoid robot.

3D TOF sensor (SR-4000)		Humanoid robot system	
Pixel array size	176 × 144	Dimension	300mm(W) × 600mm(H) × 200mm(D)
Modulation frequency	30MHz		
Non ambiguity range	5.0m	DOF	23 DOF
Field of view	44° × 35°	Sensor	1 TOF
Dimensions	65 × 65 × 68		1 Webcam

Table 3 lists the specifications for our humanoid robot system.

The height of the designed humanoid robot is approximately 600mm. To reduce the weight, the body is made of aluminum materials. Each joint is driven by the RC servo motor that consists of a DC motor, gears, and a simple controller. Our humanoid robot also has 23 Degree of Freedom (DOF) and two different vision systems: a 3D TOF camera (SR-4000) and a webcam camera.

Fig. 6 shows the GUI of the designed humanoid robot system. As shown in Fig. 6, the GUI consists of four sections: the webcam image, the TOF camera image, the 3D PEM, and the 3D VR image. The webcam image and the TOF camera image come from the webcam and 3D TOF camera, respectively, in real time. The 3D PEM image is generated by using the MDGHM-SIFT algorithm. Finally, the 3D VR image, which is produced using the OpenGL library [14], shows the analyzed environmental information.

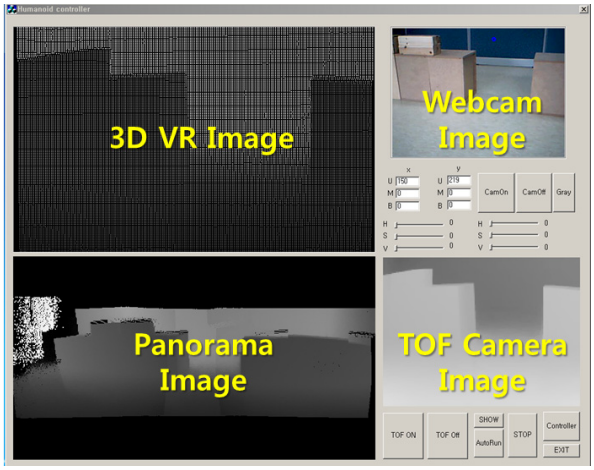

Fig. 6. GUI for the designed Humanoid Robot.

3.2 Experimental setup

The designed humanoid robot system uses a ToF camera (SR-4000), which produces disparity images with a resolution of 176× 144 pixels at 30 frames per second (fps). To test our local planning method, we set up an environment containing obstacles of different avoidance space. Fig. 7 shows the experimental environment.

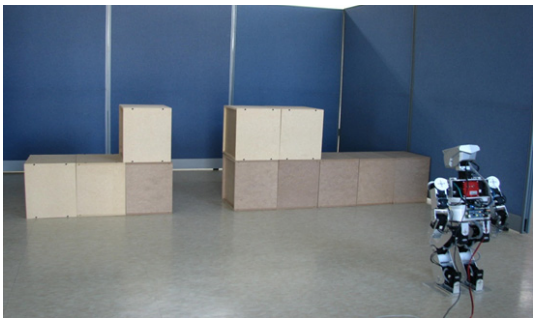

Fig. 7. Experimental environment.

The experiment space is 2.5m × 3m with artificial obstacles which have 32cm(W) × 32cm(H) × 24cm(D). These obstacles were combined into various shapes with different widths and avoidance spaces.

3.3 Experiment results for obstacle analysis

We estimated the obstacle sizes using the PEM image with the MDGHM-SIFT algorithm. Then we compared the accuracy of those sizes against obstacle size estimates obtained by using the PEM image with the SIFT algorithm.

For this experiment, we used obstacles with different widths: 71.3cm, 95.4cm, 119.5cm, and 142.8cm. Fig. 8 shows sample PEM images generated by using two consecutive images. Table 4 shows the results of size

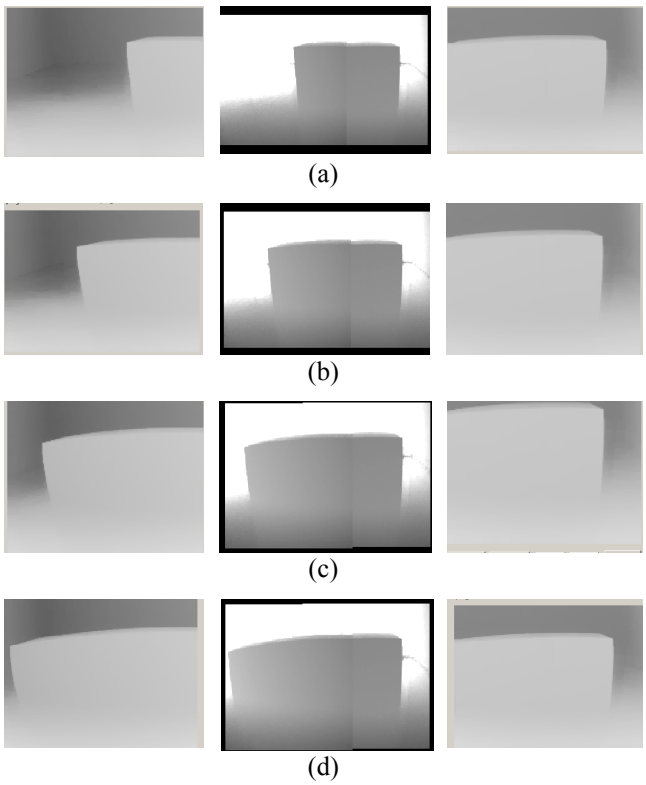

Fig. 8. Sample PEM images made by using two consecutive images at 105 cm.

Table 4. Experimental results for size estimation using the SIFT and the MDGHM-SIFT algorithm

Method	Distance (True)	Distance (Robot)	ER (%)	Width (True)	Width (Robot)	ER (%)
MDGHM-SIFT	105	105.8	0.76	71.3	71.68	0.46
				95.4	95.77	0.39
				119.5	118.42	-0.91
				142.8	142.49	-0.22
	129	129.2	0.19	71.3	69.43	-2.68
				95.4	97.11	1.76
				119.5	119.24	-0.21
				142.8	139.53	-2.34
SIFT	105	105.75	0.71	71.3	77.31	8.42
				95.4	100.88	5.43
				119.5	121.01	1.41
				142.8	142.49	-0.22
	129	130	0.78	71.3	78.04	9.45
				95.4	101.38	5.89
				119.5	123.45	3.36
				142.8	142.15	-0.46

estimation using the SIFT and the MDGHM-SIFT for various distance and size.

As shown in Table 4, the MDGHM-SIFT-based PEM performed better than the SIFT-based PEM when estimating obstacle size.

3.4 Experiment results for obstacle avoidance

We evaluated our method for accuracy using the FAMS under various environment conditions by testing the selection and control performance with various obstacle configurations. The humanoid robot walks and stops when it encounters the obstacle within a fixed or defined distance, then it calculates the decision factors to avoid obstacles.

First, we tested the FAMS for obstacle avoidance while the humanoid robot walks. Table 5 shows the experimental results for motion selection using a confusion matrix.

Ten thousand random values for obstacle size and avoidance space were used as the input, and the output, which is composed of two basic motions, is selected in each situation. As shown in Table 5, the FAMS system makes good decisions at impressive rates, 97.84% (9784/10000) for SS motion, 98.6% (9860/10000) for SF motion, 98.25% (9825/10000) for RS motion, 99.01% (9901/10000) for RF motion, 98.71% (9871/10000) for TS

Table 5. Experimental results for avoidance motion selection using Fuzzy system

Situation	SS	SF	RS	RF	TS	TF	ST
SS	9784	0	117	0	0	0	99
SF	24	9860	0	116	0	0	0
RS	66	0	9825	0	0	0	109
RF	0	65	34	9901	0	0	0
TS	0	0	27	0	9871	0	102
TF	0	0	0	34	28	9938	0
ST	17	0	2	0	18	0	9933

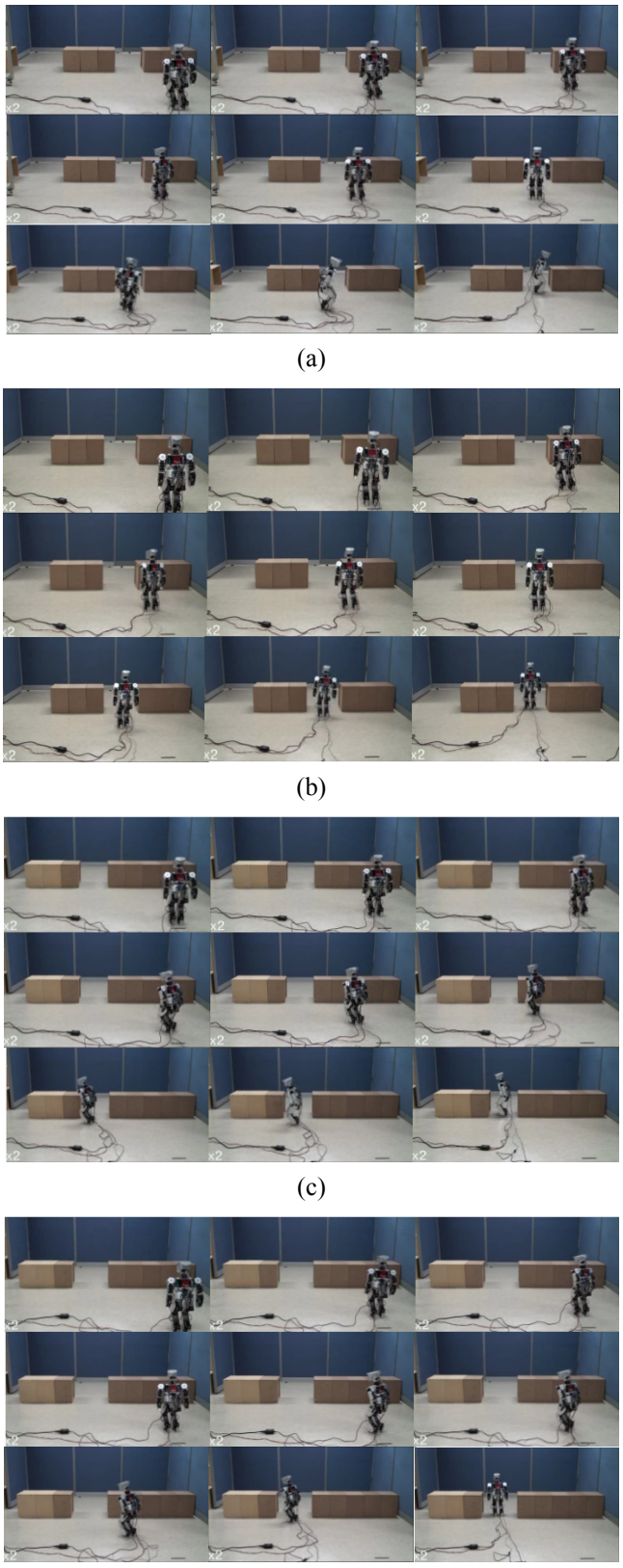

(a) (b) (c) (d)

Fig. 9. Experimental Results under various obstacle conditions: (a) SS motion type; (b) SF motion type; (c) RS motion type; (c) RF motion type.

Table 6. Experimental results for obstacle avoidance walking test

Avoidance Motion	Trials	Success	Accuracy (%)	Avg. Time (sec)
SS	15	13	87	128
SF	15	14	93	102
RS	15	12	80	120
RF	15	13	87	110
TS	15	11	73	124
TF	15	12	80	113

motion, 99.38% (9938/ 10000) for TF motion, and 99.33% (9933/10000) for ST motion.

Second, we tested the selection and control performance by using various obstacle configurations with different obstacle widths and avoidance spaces and by making fifteen attempts with each configuration. Experimental results are shown in Table 6 and Fig. 9.

If the humanoid robot arrived at the destination we defined, we considered the walking test as successful. On the other hand, if the humanoid robot collided with an obstacle or got lost in the path, we considered it as a failure. . As shown in Table 6, the experiment proves that the proposed method produces high success rates even without using any optimal control method for walking. To improve the success rate of a humanoid robot system, a vision-based adaptive walking control method can be added in future works.

Fig. 9 shows the image sequences for results under SS, SF, RS, RF conditions respectively. As shown in Fig. 9, the results show the good avoidance performance because the width of obstacles is reasonable for the humanoid robot.

4. Conclusion

In this paper, we introduced the 3D vision-based local path planning system to avoid obstacles for humanoid robot. The proposed method is based on the PEM using MDGHM-SIFT algorithm, vision based CM and FAMS systems. The PEM image can be a solution for overcoming the FOV problem that may be a major cause of the incorrect decision in walking control or perception of environment. Vision-based CM system decides the avoidance direction of a humanoid robot to avoid the obstacles through considering the environment condition such as the distribution of obstacles, the distance from the humanoid robot to obstacles and size of each obstacle. These systems don't need the global path planner which has all information regarding the obstacle location and path information in advance. Finally, FAMS system dynamically decides the avoidance motion type depending on the obstacle conditions using the visual information obtained by the PEM image. From the experimental results, we can know that our proposed methods are useful for humanoid robots in real environment.

Acknowledgements

This research was supported by the Basic Science Research Program through the National Research Foundation of Korea (NRF) funded by the Ministry of Education, Science, and Technology (Grant No. 2011-0010579).

References

[1] M. Yagi and V. Lumelsky, "Biped Robot Locomotion in Scenes with Unknown Obstacles," Proceedings of IEEE International Conference on Robotics and Automation (ICRA), pp. 375-380, 1999.

[2] J. J. Kuffner, K. Nishiwaki, S. Kagami, M. Inaba, H. Inoue, "Footstep Planning Among Obstacles for Biped Robots," Proceedings of IEEE/RSJ International Conference on Intelligent Robots and Systems (IROS), pp. 500-505, 2001.

[3] J. Chestnutt, M. Lau, G. Cheung, J. Kuffner, J. Hodgins, T. Kanade, "Footstep Planning for the Honda ASIMO Humanoid," Proc. of the 2005 IEEE Inter-national Conference on Robotics and Automation, 2005, pp. 629-634.

[4] P. Michel, J. Chestnutt, J. Kuffner, T. Kanade, "Vision-guided humanoid footstep planning for dynamic environments," 5th IEEE-RAS International Conference on Humanoid Robots, 2005, pp. 13-18.

[5] O. Stasse, B. Verrelst, B. Vanderborght, K.Yokoi, "Strategies for Humanoid Robots to Dynamically Walk Over Large Obstacles," IEEE Transactions on Robotics, Vol. 25, No. 4, Aug. 2009, pp. 960-967.

[6] F. Kanehiro, T. Yoshimi, S. Kajita, M. Morisawa, K. Fujiwara, K. Harada, K. Kaneko, H. Hirukawa, F. Tomita, "Whole Body Locomotion Planning of Humanoid Robots based on a 3-D Grid Map," Proc. of the 2005 IEEE International Conference on Robotics and Automation, April 2005, pp. 1072-1078.

[7] Y. Ayaz, A. Konno, K. Munawar, T. Tsujita, and M. Uchiyama, "Planning footsteps in obstacle cluttered environments," Proceedings of IEEE/ASME International Conference on Advanced Intelligent Mechatronics, pp.156-161, 2009.

[8] J. -S. Gutmann, M. Fukuchi, M. Fujita, "3-D Perception and Environment Map Generation for Humanoid Robot Navigation," The International Journal of Robotics Research Vol. 27, No. 10, 2008, pp. 1117-1134.

[9] B. Yang and M. Dai, "Image analysis by Gaussian-Hermite moments," Signal Processing, Vol. 91, issue 10, pp. 2290-2303, 2011.

[10] Tae-Koo Kang, Huazhen Zhang, Dong W. Kim, and Gwi-Tae Park, "Enhanced SIFT Descriptor Based on Modified Discrete Gaussian-Hermite Moment," ETRI Journal, Vol. 34, No. 4, pp.572-582, 2012.

[11] D. Lowe, "Distinctive Image Features from Scale-

Invariant Keypoints, "International Journal of Computer Vision, Vol. 2, No. 60, pp. 91-110, 2004.
[12] M. Brown and D. Lowe, "Automatic Panoramic Image Stitching using Invariant Features," International Journal of Computer Vision, Vol. 74, No. 1, pp. 59-73, 2007.
[13] K. Zhang, J. Lu, G. Lafruit; R. Lauwereins, L. V. Gool, "Robust stereo matching with fast Normalized Cross-Correlation over shape-adaptive regions," 16th IEEE International Conference on Image Processing, pp. 2357-2360, 2009.
[14] http://www.opengl.org/
[15] K. Mikolajczyk and C. Schmid, "A Performance Evaluation of Local Descriptors," IEEE Trans. Pattern Analysis and. Machine Intelligence, Vol. 27, 2003, pp. 1615-1630.
[16] L. Shapiro, and G. Stockman, Computer Vision. Prentice Hall, 2002.

Tae-Koo Kang He received his BS in applied electrical engineering, MS in visual image processing, PhD in electrical engineering from Korea University, in 2001, 2004, and 2012 respectively. He is now a research professor in School of Electrical Engineering. His research interests include computer vision, robotics, artificial intelligence, and machine learning.

Myo-Taeg Lin He received the B.S. and M.S. degrees in Electrical Engineering from Korea University, Seoul, in 1985 and 1987, respectively. In addition, he received the M.S. and Ph.D. degrees in Electrical Engineering from Rutgers University, U.S.A., in 1990 and 1994, respectively. Since 1996, he has been a Professor in the School of Electrical Engineering at Korea University. His research interests include robust control, multivariable system theory, and computer-aided control systems design. He is a Member of KIEE.

Gwi-Tae Park He received his BS, MS, and PhD in electrical engineering from Korea University, Seoul, Rep. of Korea, in 1975, 1977, and 1981, respectively. He was a technical staff member in the Korea Nuclear Power Laboratory and an Electrical Engineering faculty member at Kwangwoon University, in 1975 and 1978, respectively. He joined Korea University in 1981 where he is currently a professor in the School of Electrical Engineering. He was a visiting professor at the University of Illinois in 1984. He is a fellow of the Korean Institute of Electrical Engineers (KIEE), the Institute of Control, Automation, and System Engineers, Korea (ICASE) and advisor of the Korea Robotic Society. He is also a member of the Institute of Electrical and Electronics Engineers (IEEE) and the Korea Fuzzy Logic and Intelligent Systems Society (KFIS).

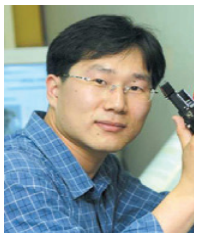

Dong W. Kim He received his PhD in electrical engineering from Korea University, Seoul, Rep. of Korea, in 2007. Dr. Kim was a post-doctoral research scholar at BISC (Berkeley Initiative in Soft Computing), University of California, Berkeley, Berkeley, CA, USA, in 2008 and the AHMCT (Advanced Highway Maintenance and Construction Technology Research Center), University of California, Davis, Davis, CA, USA, in 2009. He is now a professor in the Department of Digital Electronics, Inha Technical College. His research interests include the intelligent humanoid robot, autonomous multi-mobile robot navigation and robot intelligence based on the neuro-fuzzy system.